Materials and Design 190 (2020) 108557

Contents lists available at ScienceDirect

Materials and Design

journal homepage: www.elsevier.com/locate/matdes

# Magnetocaloric effect in bamboo-grained Ni-Mn-Ga microwires over a wide working temperature interval

M.F. Qian [a], X.X. Zhang [a,*], X. Li [a], R.C. Zhang [a], P.G. Martin [b], J.F. Sun [a], L. Geng [a], T.B. Scott [b], H.X. Peng [c]

[a] School of Materials Science and Engineering, Harbin Institute of Technology, Harbin 150001, China
[b] Interface Analysis Centre, University of Bristol, Bristol BS8 1TL, United Kingdom
[c] Institute for Composites Science Innovation (InCSI), School of Materials Science and Engineering, Zhejiang University, Hangzhou 310027, China

## HIGHLIGHTS

- Bamboo-grained Ni-Mn-Ga microwires were prepared and negligible magnetic hysteresis was attained.
- No texture was obtained in the bamboo-grained microwire at austenite state.
- Multi-variants state was obtained in each grain due to the compositional variation.
- Working temperature interval ~71 K and net refrigeration capacity ~255 J/kg under 5 T were achieved.

## GRAPHICAL ABSTRACT

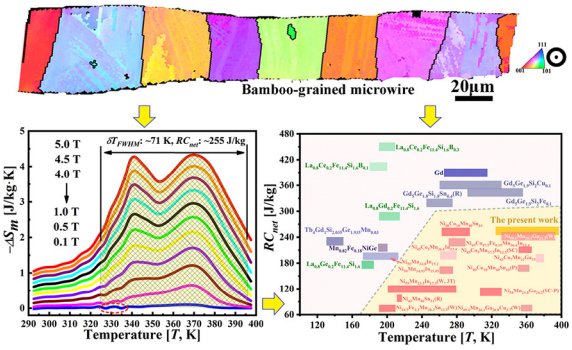


## ARTICLE INFO

*Article history:*
Received 22 September 2019
Received in revised form 26 December 2019
Accepted 7 February 2020
Available online 07 February 2020

*Keywords:*
Ni-Mn-Ga microwires
Bamboo-grained structure
Hysteresis loss
Magnetocaloric effect
Refrigeration capacity

## ABSTRACT

Bamboo-grained Ni-Mn-Ga microwire is promising for achieving considerable magnetic-field-induced strain due to less neighboring grain constraints to the twin boundary motion. Such reduction of resistance to interface motion also favors the reduction of hysteresis in magnetic refrigeration. Here, bamboo-grained Ni-Mn-Ga microwires were successfully synthesized by a melt-extraction technique and subsequent high temperature heat treatment at 1323 K for 3 h under Argon atmosphere. Corresponding microstructure, martensite transformation (MT) behaviors and magnetocaloric properties were investigated. The high specific surface area of the microwires favored the element evaporation at high temperature, leading to a heterogeneous composition state, which is responsible for the MT temperature (range) change and the multi-variants state in the bamboo-grained microwires. Nearly no magnetic hysteresis loss was obtained. The increased compositional variation led to the partial overlap of the MT and the magnetic transition, resulting in the improvement of the working temperature interval ~71 K and net refrigeration capacity ~255 J/kg under $\mu_0 H = 5$ T, which is heretofore the largest value reported in Ni-Mn-based Heusler alloys. When utilized as refrigerant in a cooling device, such small-sized microwires can increase the contacting area between the material and the heat-transfer agent, which helps the heat exchange and thus improve the refrigeration efficiency.



* Corresponding author.
*E-mail address:* xxzhang@hit.edu.cn (X.X. Zhang).

https://doi.org/10.1016/j.matdes.2020.108557

## 1. Introduction

The magnetic refrigeration technique is based on the magnetocaloric effect (MCE), which is defined as the temperature variation under adiabatic condition or entropy variation under isothermal condition via the application and removal of an external magnetic field. It is considered as a promising alternative to the traditional vapor-compression refrigeration technique due to its outstanding merits such as environmental friendliness, energy efficiency and low cost [1–6]. In the last two decades, magnetic refrigeration materials have been widely explored and investigated, mainly involving the $La(Fe, Si)_{13}$ system [7–9], $Gd_5(Si, Ge)_4$ system [10,11], Mn-Co-Ge-based alloys [12] and Ni-Mn-based Heusler type alloys [13–21], etc. Among them, considerable attentions have been paid to the off-stoichiometric Heusler type alloys, i.e. Ni-Mn-Z (Z = In, Sn, Sb, Ga), where an enhanced MCE can be attained due to the existence of a coupled first-order magnetostructural transformation [22–24].

For Ni-Mn-Ga-based alloys, large conventional MCE can be produced both in the vicinity of the first-order martensite transformation (MT) and the second-order magnetic transition [21]. Previous investigation have demonstrated that the MCE in Ni-Mn-Ga based alloys are strongly dependent on the composition since the MT and the magnetic transition can be tuned to be overlapped by tuning the chemical composition, i.e. a first-order magnetostructural transformation between a paramagnetic austenite and a ferromagnetic martensite can be achieved, giving rise to a further enhanced MCE [21]. On the other hand, the tunable transformation temperature feature also enables the possibility of designing magnetic refrigerators with working temperature close to room temperature [25]. Therefore, the study of Ni-Mn-Ga-based alloys is not only for scientific research purpose, but more importantly for practical applications.

Nevertheless, despite the advantages, several drawbacks owing to the first-order nature of transformation, such as the undesirable hysteresis and concentrated working temperature interval (*WTI*), hamper the available cooling capacity in Ni-Mn-Ga-based alloys and therefore their practical application in cooling devices. The hysteresis, which is an inevitable character of the first-order MT, is mainly related to the resistance to interface motion between martensite and austenite during transformation [26]. In this case, reducing the neighboring grain constraints, i.e. increasing the free surface of the crystal grains, through reducing the sample size, increasing the grain size [27] or directly removing the neighboring grains out of the alloys [7] was reported to be effectual. Except for the effect of cutting down the grain boundaries, an unstressed, untwined interface between the phases which favors to form martensite with low density of twins would be favorable to achieve low hysteresis as well [28]. Given these concepts, different configurations such as bulk single crystals [28], single crystalline powders [20], microwires/fibres [21,29], ribbons [30] and porous foams [7] have been introduced in many kinds of MCE materials and low thermal hysteresis during MT were successfully attained. Among them, single crystals are difficult to fabricate and porous structure would somehow "dilute" the refrigeration efficiency. Small-sized microwires and ribbons are usually easy to prepare on a large scale and the defects as well as the fine grains formed during the rapid solidification processes are favorable for the further growth of the grains, where reduced hysteresis can be expected. However, it has been reported that for bamboo-grained microwires, the rough free surface was the main obstacles of the phase boundary motion which would increase the hysteresis [31]. Besides the effect of the coarse grains, usually after certain heat treatments, the decreased defects density and released internal stress would further reduce the hysteresis [27,32]. On the other hand, with respect to the concentrated *WTI*, small-sized Ni-Mn-Ga based materials favors the element evaporation (such as Mn) during high temperature heat treatment, which enlarges the MT temperature range so that a widened *WTI* can be expected, especially when MT and the magnetic transition are partly overlapped [21].

In this context, a bamboo-grained Ni-Mn-Ga based microwire with smooth external surface would be beneficial for the hysteresis reduction and *WTI* enlargement. During the past decades, the bamboo or near bamboo-grained Ni-Mn-Ga microwires have attracted much interests, mostly concentrate on the exploration of giant magnetic-field-induced strain (MFIS) [33–35], owing to the reduced neighboring grain constraints on the twin boundary motion which makes them the closest approximation to single crystals. While few work has been reported regarding the MCE of them. In our previous work, MCE of several kinds of fine-grained Ni-Mn based microwires have been investigated and excellent MCE properties comparable or even superior to those of bulk alloys have been obtained [21,23,36,37]. Reduced hysteresis losses were achieved [21,23,36,37] and of note is that gradient composition distribution can be obtained in Ni-Mn-Ga microwires due to the element evaporation on the wire surface, which significantly enlarged the *WTI* [21].

Here, with the aim to further reduce the neighboring grain constraints, bamboo-grained Ni-Mn-Ga microwires were successfully synthesized by a melt-extraction technique and subsequent high temperature heat treatment at 1323 K for 3 h. The microstructure, MT behaviors and MCE properties were investigated. The results showed that the magnetic hysteresis was negligible while the thermal hysteresis loss of the bamboo-grained microwires was slightly increased. On the other hand, the increased compositional variation in bamboo-grained microwires led to the partial overlap of the MT and the magnetic transition, resulting in the improvement of the *WTI* ~71 K and net refrigeration capacity ~255 J/kg under 5 T.

## 2. Experimental methods

Ni-Mn-Ga alloy ingots with nominal composition of $Ni_{50.6}Mn_{28.0}Ga_{21.4}$ (atomic percent) were prepared by induction melting pure Ni (99.99%), Mn (99.99%) and Ga (99.99%) in an Argon atmosphere and casting into a copper mold with a diameter of 9 mm. Ni-Mn-Ga microwires were fabricated by a modified melt-extraction method and the detailed fabrication process can be found elsewhere [38]. Thereafter, the as-extracted microwires were sealed in a quartz tube accompanied with several Ti sheets, evacuated and back-filled with 0.5 atm. of pure Ar gas at room temperature, stepwise heat-treated at 1323 K for 3 h, 998 K for 2 h, 973 K for 10 h, 773 K for 20 h and then furnace-cooled to room temperature. The Ti sheets were used to absorb the residual oxygen in the tube. As for the stepwise heat treatment, "1323 K for 3 h" is a grain growth process to attain the bamboo-grained structure, "998 K for 2 h and 973 K for 10 h" are aim to improve the atomic order and "773 K for 20 h" is to release the internal stresses formed during the melt-extraction process [32,39].

The compositions are determined by using a scanning electron microscope (SEM) equipped with an X-ray energy dispersive spectroscopy (EDS) using 20 kV voltage, 97 μA emission current, 10 mm work distance and 50 μA probe current and >60 s data acquisition time duration. The precision of the EDS was calibrated with chemical analysis results (ICP-OES) to be less than 0.5%. The surface and fracture morphologies of the microwires were examined using the SEM. EBSD was used to determine the orientation of the bamboo grains. The EBSD wire sample was firstly mounted in conductive resin (Struers Polyfast), grinded, manually polished and finally automatically polished in a Buehler® Vibromet® vibratory polisher for 24 h. A homemade in-situ heating stage (Interface Analysis Centre, University of Bristol, U.K.) was used for sample

heating for high temperature EBSD measurement. EBSD analysis was performed in a Zeiss Sigma™ HDVP field Emission SEM with Gemini electron source and a Digiview 3 high speed EBSD camera from EDAX™. A consistent 30 kV accelerating voltage, 100 μA beam current, 120 μA aperture and 16 mm working distance were used throughout the experiment.

The microstructure of the microwires was examined in a Tecnai $G^2$ F30 transmission electron microscope (TEM). X-ray diffraction (XRD) tests were performed on a Philip X'pert Pro instrument with Cu Kα radiation ($\lambda = 1.54$ Å) for phase identification. A TTK 450 low temperature chamber was used for sample cooling for low temperature phase identification. The scan speed was 0.005°/s with a step size of 0.02°. MT temperatures and enthalpy changes of the microwires were measured by a TA Q200 differential scanning calorimetry (DSC) with a cooling and heating rate of 5 K/min. The isofield magnetization (*M-T*) and isothermal magnetization (*M-H*) measurements were carried out by using a vibrating sample magnetometry (VSM) in a physical property measurement system (PPMS) of Quantum Design. In order to fit the sample holder of the equipment, a bundle of wires (~30 wires) with an average length of 5 mm were prepared and used for the magnetic measurements, where the microwires were arranged parallel with each other in a Teflon tube with an outer diameter of 3 mm. The magnetic field was applied parallel to the direction of the wire axis. *M-T* curves were recorded under 0.02 T with a cooling and heating rate of 5 K/min. *M-H* curves were measured on heating procedure at different temperatures from 290 to 400 K under an external magnetic field up to 5 T. The magnetic entropy change $\Delta S_m$ was calculated from the *M-H* curves based on the Maxwell relation.

## 3. Results and discussion

### 3.1. Microstructural characterization

The morphologies of the as-extracted and annealed microwires are presented in Fig. 1. Microwires with diameter ~30–80 μm and length ~2–20 cm have been successfully prepared on a large scale by the melt-extraction method, as shown in Fig. 1a. The as-extracted microwires exhibit noticeable metallic luster. The details regarding the morphology and grain structure of the as-extracted microwires have been reported in our previous work [40]. Characteristic of transcrystalline fracture has been observed in the "D" shaped cross-section, as shown in Fig. 1b, showing improved ductility in the present fine-grained microwires.

After high temperature grain growth heat treatment, the grains grow significantly and bamboo-grained structure has been successfully attained with smooth external surfaces, where all the grains span the entire wire cross-section with grain boundaries generally perpendicular to the wire axis, as shown in Fig. 1c and d. The length of the bamboo grains along the wire axis varies from tens to hundreds of microns, mainly due to the varied original microstructure, such as the different vacancy [41] or internal stress [42] distribution, in the as-extracted microwires. The inset in Fig. 1c shows a magnification of the bamboo

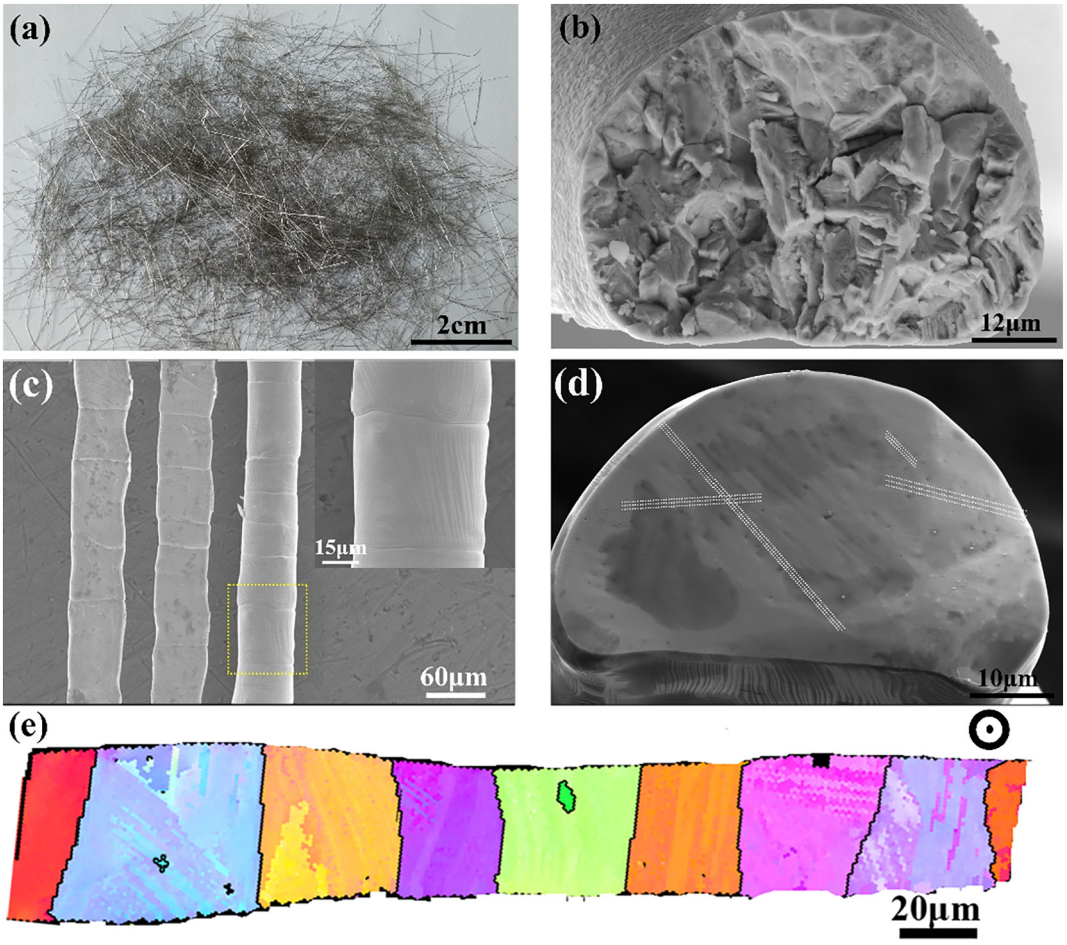


**Fig. 1.** Morphologies of (a, b) as-extracted and (c–e) bamboo-grained microwires. (a) Macroscopic morphology, (b) fracture cross-section, (c) outer surfaces, (d) cross-section with single grain, (e) high temperature EBSD map using the IPF normal direction coloring scheme. The inset in (c) displays the magnification of the bamboo grains from the yellow box. The white dash lines in (d) demonstrate the contours of the martensite twins, showing several different martensite variants. (For interpretation of the references to color in this figure legend, the reader is referred to the web version of this article.)

grains. Martensite plates span across the full length of the grain can be observed on the surface of the wire, indicating the martensite state at room temperature. However, the boundaries of the twins are not clear and straight. Besides, white dash lines in Fig. 1d demonstrate the contours of the martensite twin boundaries on the cross-section of the bamboo-grained microwire. Several different variants with fine twin lamella in one grain can be observed, which is very much different from that in the near bamboo-grained Ni-Mn-Ga microwires of our prior work, where coarse twin variant with single twin lamella thickness up to 6 μm covering the entire cross-section of the wire was attained [35]. The multi-variants state in the present work may be related to the increased compositional variation after higher temperature heat treatment. This will elucidate in detail later in this paper.

Fig. 1e demonstrates the high temperature EBSD orientation map (longitudinal-section) with normal direction coloring scheme of the bamboo-grained microwire recorded at ~353 K (at austenite state). Within the map, bamboo-grained structure with grain length from 20 to 60 μm can be observed. It has been reported in our previous work that in the as-extracted microwires at austenite state, the grains tend to form a fan-like texture with grains mostly grow along the ⟨001⟩ crystal orientation controlled by the heat transfer during fabrication [39]. However, no obvious preferred grain orientation can be observed in the bamboo-grained microwire here, indicating that the texture formed during fabrication cannot be inherited after grain growth. It is worth noting that due to certain composition and size differences between the as-extracted microwires, complete bamboo-grained structure cannot be guaranteed for all wires after such heat treatment. To some extent, it has been confirmed in our work that finer microwires are easier to achieve bamboo-grained structure than that of the thicker ones.

Compositions of the microwires both on the surface and the cross-section (10 wires on the surface and 10 wires on the cross-section each) have been measured. The results show that the inner and outer compositions of the as-extracted microwires vary little while those of the bamboo-grained ones show relatively large differences. Therefore, the average compostion of the as-extracted and both inner and outer average compostions of the bamboo-grained microwires are listed in Table 1, respectively, and all standard deviations are given. Due to the high specific surface area of the microwires, after heat treatment, in the exterior of the microwires, the content of Ga and Mn element decreases by 0.5 and 1.0 at.% when compared with the as-extracted microwires, respectively, giving rise to the increased Ni content. In addition, the increased standard deviation values of the bamboo-grained microwires, as shown in Table 1, elucidates that the high temperature heat treatment markedly deteriorates the homogeneity of the compositions in microwires. One can notice that due to the higher evaporation tendency of Mn at high temperature, Mn content becomes lower on the surface than on the inside of the bamboo-grained microwires, which is consistent with our previous work in chemical ordering annealed Ni-Mn-Ga microwires where gradient Mn distribution state with depletion of Mn near the surface layer of the wire cross-section was obtained [21]. Owing to the increased compositional variation, widened MT temperature range can be expected. Furthermore, considering the inhomogeneity of the composition within the cross-section area of the bamboo-grained microwire, different part of the cross section would have different MT behaviors since the MT temperatures in Ni-Mn-Ga alloys are strongly dependent on the compositions [25]. In this context, not only will the MT range increase, different martensite twin structure also can be formed at different parts of the wire, leading to the complexity of the twin structure in the present work, as mentioned earlier in Fig. 1c and d.

**Table 1**
Compositions of the Ni-Mn-Ga microwires before and after grain growth heat treatment.

| Microwire | Location | Composition (at.%) | | | | | |
|---|---|---|---|---|---|---|---|
| | | Ni | ΔNi | Mn | ΔMn | Ga | ΔGa |
| As-extracted | Average | 50.6 | 0.4 | 28.8 | 0.3 | 20.6 | 0.4 |
| Annealed | Interior | 51.3 | 0.8 | 28.4 | 0.8 | 20.3 | 0.7 |
| | Exterior | 52.1 | 0.8 | 27.8 | 0.8 | 20.1 | 0.9 |

Fig. 2 depicts the low temperature X-ray diffraction (XRD) patterns of the as-extracted and bamboo-grained microwires at their complete martensite state (263 K). The patterns of the as-extracted microwires (as shown Fig. 2a) can be indexed as a 7-layered modulated martensite (7M martensite). After grain growth heat treatment, 5-layered modulated martensite (5M martensite) showed up thus formed a mixed state of both 5M and 7M martensites, as revealed by the splitting of the diffraction peaks presented in the inset of Fig. 2b. By the whole pattern fitting analysis, the 7M martensites in both microwires are determined to be a monoclinic incommensurate superstructure [43] with lattice constants a = 0.426 nm, b = 0.550 nm, c = 4.249 nm, β = 93.4° and a = 0.429 nm, b = 0.521 nm, c = 4.402 nm, β = 94.3° for the as-extracted and bamboo-grained microwires, respectively. Yet, due to the lack of peak data, exact crystal structure information of the 5M martensite cannot be evaluated in the present work. Nevertheless, one can observe that the lattice parameters of 7M martensite have been changed after heat treatment. Here, we believe the discrepancy is twofold. One is due to the decreased defects density and released internal stress, and the other is the increased compositional variation. These factors also contribute to the changes in martensite types. It has been reported by Segui et al. [44] that the 7M martensite is more stable than 5M martensite, where upon applying increasing stress, the parent austenite phase firstly transforms to 5M and then to 7M, or directly transform to 7M in samples with higher internal stresses. That is to say, the internal stress formed during rapid solidification in as-extracted microwires favored the formation of 7M. Whereas, after high temperature heat treatment thus internal stress relaxation, 5M showed up again. On the other hand, it has been confirmed that the martensite types of Ni-Mn-Ga alloys are strongly dependent on the composition [45], thus, the compositional variation may contributes to the martensite phase change as well. Formation of different types of martensites via intermartensite transformation was reported to be beneficial for obtaining better MCE with enlarged *WTI* in Ni-Mn-Ga alloys [46].

Fig. 3 shows the TEM bright field images and corresponding electron diffraction patterns of the as-extracted and bamboo-grained microwires at room temperature. As shown in Fig. 3a and the inset, both austenite and martensite can be observed in the as-extracted microwire with clear phase boundary between them. The corresponding electron diffraction pattern showing six extra diffraction spots between two main spots, as marked by red arrows, demonstrates the 7M martensite, which is consistent with the XRD result. It is worth noting that certain amount of dislocations can be found in austenite region, implying improved ductility of the as-extracted microwires, which is considered to be related to the rapid solidification process during melt-extraction. In the meantime, martensite displays obvious twin lamellar structure and the movement of the martensite/austenite interface, to some extent, has been halted inside the grain, indicating large resistance during transformation. After high temperature heat treatment, as shown in Fig. 3b and the inset, more regularly arranged 5M martensite twin lamellar structure with twin boundaries strictly parallel with each other can be observed. The width of each lamella is around 120 nm and no dislocation can be seen within the observation area. The absent of the 7M martensite in bamboo-grained microwires mainly due to the limited TEM sample size.

### 3.2. Characteristics of martensite transformation

To further investigate the MT behaviors, both heating and cooling DSC and low field (0.02 T) isothermal magnetization $M(T)$ curves of the as-extracted and bamboo-grained microwires are measured and recorded, as shown in Fig. 4a and b, respectively. It is worth noting that

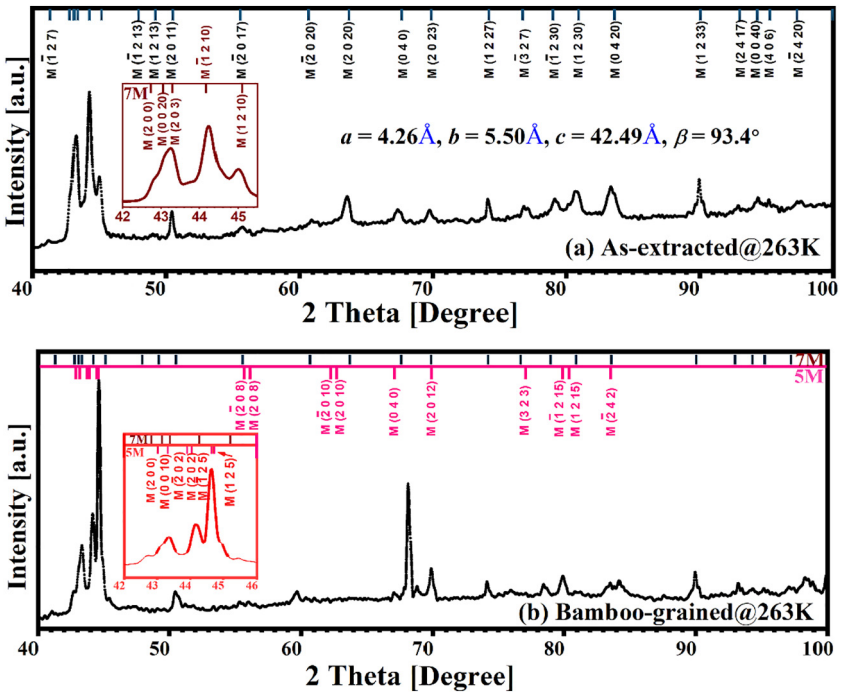


**Fig. 2.** Low temperature (263 K) XRD patterns of the (a) as-extracted and (b) bamboo-grained microwires.

heat flow fluctuations can be observed from the DSC curves in the bamboo-grained microwires. What's more, the 1st derivation of the $M(T)$ curves, as shown in the inset ② in Fig. 4b, also shows similar fluctuation feature during MT transformation. This phenomenon is mainly due to the increased compositional variation after high temperature heat treatment, which leads to the MT temperature discrepancy either among different parts of one single wire or between different wires. Probably owing to the fluctuation of the curves, no significant intermartensite transformation behavior, normally characterized by two successive peaks, exists in DSC curves or the 1st derivation of the $M(T)$ curves of the bamboo-grained microwires, where 5M and 7M martensite have been confirmed to be coexisted, as shown in Fig. 2b. Besides, sharp peak (marked with blue circle) close to $T_c$, mainly relate to high internal stress anisotropy formed during rapid solidification [47], is found in the as-extracted microwires, as shown in Fig. 4b, confirming the existence of high internal stress. This phenomenon vanishes with heat treatment, mainly due to the stress relief annealing process [32].

The martensite start/finish temperatures, austenite start/finish temperatures ($M_s$, $M_f$, $A_s$, $A_f$) and the Curie temperature ($T_c$) derived from both DSC and $M(T)$ curves are summarized and listed in Table 2. The MT temperatures are determined based on the conventional tangent method, as demonstrated in Fig. 4a. The MT temperature range is the difference between the start and finish temperatures ($M_s$-$M_f$, $A_s$-$A_f$). The transformation thermal hysteresis loss is defined as the peak to peak value ($A_p$-$M_p$), where $M_p$ and $A_p$ represent the peak temperatures from DSC or the 1st derivation of the $M(T)$ curves upon cooling and heating, respectively. As shown in Table 2, both forward and reverse MT temperatures and $T_c$ shift towards higher temperatures with increased transition range and peak to peak thermal hysteresis after high temperature heat treatment. Obviously, the increased MT temperatures of the bamboo-grained microwires, is related to the compositional variation, release of the internal stresses and the increased size of the grains. The raise of $T_c$ value from 351.7 K to ~370 K (370.5 K from DSC and 369.3 K) elucidates the enhancement of the magnetic

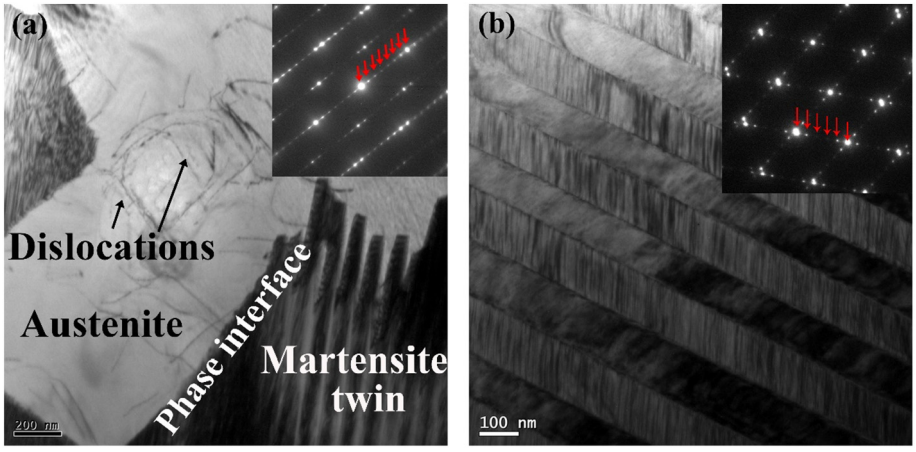


**Fig. 3.** TEM bright field images and corresponding electron diffraction patterns of the (a) as-extracted and (b) bamboo-grained microwires. (For interpretation of the references to color in this figure, the reader is referred to the web version of this article.)

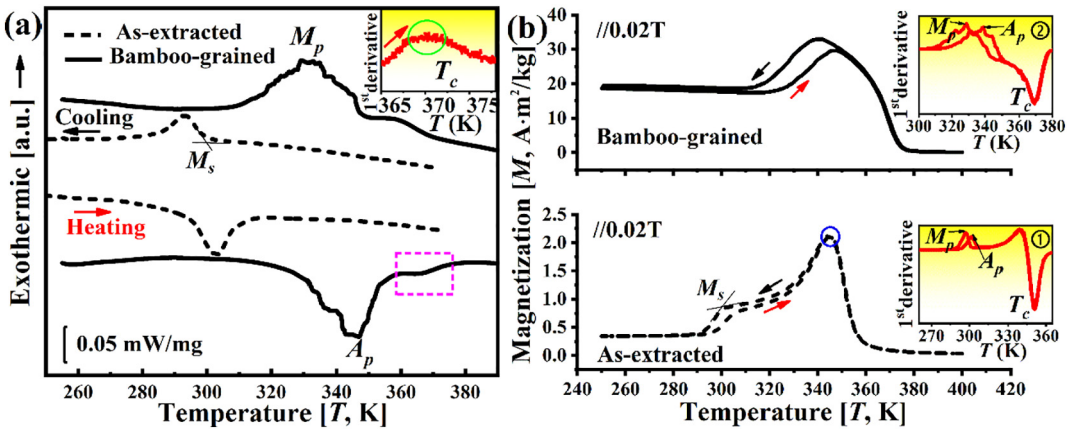


**Fig. 4.** Heating and cooling (a) DSC curves and (b) isofield magnetization $M(T)$ curves (recorded at $\mu_0 H = 0.02$ T) of the as-extracted and bamboo-grained microwires. The inset in (a) shows the 1st derivative of the DSC curves around $T_c$ (ranging from 365 to 379 K) of the bamboo-grained microwires. The inset ① and ② in (b) represent the 1st derivative of the corresponding $M(T)$ curves of the as-extracted and bamboo-grained microwires. (For interpretation of the references to color in this figure, the reader is referred to the web version of this article.)

property after heat treatment, mainly due to the chemical ordering annealing process [32]. The magnetization results, as shown in Fig. 4b, where the magnetization value under 0.02 T of the bamboo-grained microwires is much higher than that of the as-extracted ones, also confirmed the enhanced magnetic property.

Take the DSC data for instance, one can easily observe from Table 2 that the MT temperature ranges during the forward and reverse transformation change from 14.2 and 15 K to 37 and 34.9 K after high temperature heat treatment. Normally, the reduced internal stress and the increased grain size would lead to the reduction of the stored elastic strain energy $E_e$ during MT since in bamboo-grain microwires the transformation strains can take place against the atmosphere as the phase interface travels the specimen [26]. As a result, reduced energy barrier leads to less undercooling needed for further transformation, i.e. decreases the transition range. However, as mentioned before, the increased variation of the composition gives rise to the MT temperature discrepancy of the bamboo-grained microwires, as if it was a composite composed of many different types of microwires, giving rise to the markedly enlarged MT temperature range, which favors the enlargement of the refrigeration *WTI*.

As demonstrated in Fig. 3a, we believe that the halted martensite/austenite interface indicates large resistance during transformation. As is well known, one of the energy dissipative processes during MT is in the form of frictional work, which is spent overcoming the resistance to interfacial motion, and is related to the density of obstacles or defects at the transformation front [26,31]. Therefore, the existing high internal stress and dislocations, in the austenite phase of as-extracted microwires, as demonstrated in Figs. 4b and 3a, are responsible for the large resistance. Thus, high transformation hysteresis should be expected in as-extracted microwires, if consider the factor of internal friction dissipation alone. It stands to reason that after high temperature heat treatment, the reduction of the defects and internal stresses would reduce the internal friction dissipation, thus, reduce the transformation hysteresis. However, as shown in Table 2, the hysteresis values increased from 9.6 to 13.0 K derived from DSC and 4.4 to 9.5 K from $M(T)$ curves, respectively. The reason is related to another energy dissipative process, the $E_e$ dissipation [26]. As mentioned before, $E_e$ tends to release during the forward transformation in bamboo-grained microwires, whereas, $E_e$ is the driving force for the reverse transformation. As a result, less driving force exists, leading to the delay in the reverse transformation, which widens the transformation thermal hysteresis. On the other hand, it has been reported that the increase of thermal hysteresis in coarse grained sample is largely related to the lack of nucleation site of martensite due to the reduction of grain boundary area and defects density after high temperature annealing [48], although some also said that the decreased defects density and released internal stress further reduced the hysteresis [27,32]. Furthermore, prior work by Chen et al. elucidated that, for bamboo grained SMA microwires, the rough free surface provides the main obstacles for the interface motion [31]. Actually, no definition for a "smooth" surface has been made, thus, the free surface of microwire may degrades the useful mechanical work into frictional work and widens the transformation hysteresis in the present work as well. Nevertheless, it has also been confirmed in Ni-Mn-Ga single crystalline [49] and foams [50,51] that the reduction of grain boundary areas decreases the constraints provide by the neighboring grains, thus, favors the interface motion and reduces the hysteresis. In addition, some work [28] indicates that an unstressed, untwined interface between martensite and austenite would cause the minimum hysteresis. However, as shown in the cross-section (Fig. 1d) and TEM result (Fig. 3b) in the present work, complex twin distribution and fine martensite twin lamella with width of ~120 nm have weakened this effect. In conclusion, the factors that influence the transformation thermal hysteresis of the bamboo-grained microwires are multi-fold, and the combination of all the effects above leads to the current hysteresis state. Recently, a multi-caloric cooling cycle combine the magneto- and elasto-caloric effects, which exploits the thermal hysteresis has been demonstrated in Ni-Mn-In alloys [52]. With both excellent magnetocaloric [20,21] and elastocaloric

**Table 2**
Martensite transformation temperatures, enthalpy change values and Curie temperatures of as-extracted and bamboo-grained microwires.

| Material state | Method | $M_s$ | $M_p$ | $M_f$ | $A_s$ | $A_p$ | $A_f$ | $T_c$ | Hysteresis | $\|Q_c\|$ | $\|Q_h\|$ |
|---|---|---|---|---|---|---|---|---|---|---|---|
| | | K | | | | | | | | J/g | |
| As-extracted | DSC | 299.8 | 293.6 | 285.6 | 294.7 | 303.2 | 309.7 | – | 9.6 | 4.3 | 4.8 |
| | VSM | 302.3 | 297.5 | 294.2 | 299.3 | 301.9 | 305.1 | 351.7 | 4.4 | – | – |
| Bamboo-grained | DSC | 347.5 | 332.1 | 310.5 | 322.9 | 345.1 | 357.8 | 370.5 | 13.0 | 8.9 | 9.2 |
| | VSM | 341.0 | 329.6 | 314.2 | 324.1 | 339.1 | 348.9 | 369.3 | 9.5 | – | – |

effect [53], multi-caloric cooling cycle may be realized in Ni-Mn-Ga alloy as well. In this context, large thermal hysteresis may not be a main obstacle hindering the practical application in Ni-Mn-Ga alloys.

In addition, $|Q_c|$ and $|Q_h|$ are the enthalpy change values of the microwires during forward and reverse transformation, respectively. As shown in Table 2, the enthalpy nearly doubled after heat treatment. The transformation entropy change $\Delta S_{tr}$ can be estimated as $\Delta S_{tr}^{endo} = |Q_h|/A_p$ and $\Delta S_{tr}^{exo} = |Q_c|/M_p$ during heating and cooling, respectively. According to the DSC results, $\Delta S_{tr}^{endo}$ and $\Delta S_{tr}^{exo}$ can be calculated as ~15.8 and ~14.6 J/kg·K for the as-extracted and ~26.7 and ~26.8 J/kg·K for the bamboo-grained microwires, respectively.

### 3.3. Magnetic properties and magnetocaloric effect

In order to evaluate the magnetic properties and magnetocaloric effect (MCE) of the bamboo-grained microwires, isothermal magnetization curves $M(H)$ were measured, as shown in Fig. 5a. The isothermal entropy change $\Delta S_m$ was calculated based on the $M(H)$ curves by using the discretized Maxwell equation (Eq. (1)).

$$\Delta S_m = \sum_j \frac{M_{i+1} - M_i}{T_{i+1} - T_i} \Delta H_j \tag{1}$$

The validity and reliability of the Maxwell relation in evaluating the MCE of Ni-Mn-Ga alloys has been confirmed due to its weak magnetoelastic coupling during MT [54]. Fig. 5b plotted the temperature dependence of $\Delta S_m$ at different magnetic fields up to 5 T, with an increment of 0.5 T, of the bamboo-grained microwires. Saddle-like shape of the $\Delta S_m(T)$ curves were obtained, showing two peak values of ~4.3 J/kg·K around MT and ~4.4 J/kg·K around $T_c$, respectively, and a transition region between them with minimum value of 3.7 J/kg·K under 5 T. Similar shape has been reported in our previous chemical ordered Ni-Mn-Ga microwires with partly coupled magnetostructural transformation [21], meaning that the combination effect of the widened MT temperature range, increased MT temperature and the almost intact $T_c$ after high temperature heat treatment also exhibit a partly coupled magnetostructural transformation state. This partly coupled state gives rise to the significant enlarged refrigeration *WTI* ($\delta T_{FWHM}$, full width at half maximum of the $\Delta S_m(T)$ peaks at 5 T) of ~71 K in the present bamboo-grained microwires, which is superior to that in the chemical ordered microwires [21].

In addition, similar positive $\Delta S_m(T)$ peaks, as marked with red dashed ellipse in Fig. 5b, are also found at lower magnetic fields. According the Maxwell relation, the intersections between $M(H)$ curves at lower fields, as demonstrated in red ellipse in Fig. 5a, explains the positive to negative transition behavior of the $\Delta S_m(T)$ peaks here. This phenomenon is common and mostly related to the difficulty in magnetizing the preferentially oriented magnetic domains at lower magnetic field and lower temperature. Differently, not one but two positive peaks were attained in the present work, which is mainly due to the increased compositional variation of the bamboo-grained microwires where the magnetic properties of the microwires vary with composition as well.

On the other hand, in order to evaluate the MCE, the magnetic hysteresis loss, which is determined from the area between the $M(H)$ curves recorded during magnetization and demagnetization, should be considered. Here, according to the field-up and field-down isothermal magnetization $M(H)$ curves, as shown in Fig. 5a, almost no magnetic hysteresis can be observed. As mentioned earlier, the resistance to the interface motion was reduced after high temperature heat treatment. Therefore, the present magnetic hysteresis state might be related to the reduced resistance to the magnetic domain wall motion in the bamboo-grained microwires.

For practical applications, the refrigeration capacity (*RC*) value, which requires not only a large $\Delta S_m$, but also widened *WTI* and small magnetic hysteresis loss, is of great importance. The *RC* value is a measure of transport of thermal energy between hot and cold reservoirs in one ideal refrigerate cycle, which can be calculated by integrating the $\Delta S_m(T)$ curve over the $\delta T_{FWHM}$ range ($T_{cold}$-$T_{hot}$) (Eq. (2)).

$$RC(\delta T, H) = \left| \int_{T_{cold}}^{T_{hot}} \Delta S_m(T, H) dH \right| \tag{2}$$

The net refrigeration capacity ($RC_{\text{net}}$) value, which is more reasonable to evaluate the cooling efficiency, can be calculated by subtracting the magnetic hysteresis loss from the *RC* value. Due to the vanished magnetic hysteresis, the $RC_{\text{net}}$ value for the present bamboo-grained microwires is calculated to be ~255 J/kg at 5 T, which is heretofore the largest value reported in Ni-Mn-based Heusler alloys.

The $RC_{\text{net}}$ values as a function of temperature under 5 T for the most studied magnetocaloric materials (Ni-Mn-based [20,21,23,37,55–62], Gd-Si-Ge-based [63–65], La-Fe-Si-based [66,67], Mn-Fe-Ni-Ge compounds [68] and Gd [3]) and the present bamboo-grained microwires are schematically illustrated in Fig. 6, permitting a fast comparison. The width of each rectangle stripe stands for the *WTI*. Obviously, the present bamboo-grained microwires exhibits the largest *WTI* among all types of materials and the $RC_{net}$ value is the highest among all the Ni-Mn-based particles [20,55], microwires [21,23,37,60], ribbons [40,61], single crystals [57] as well as bulk alloys [56,58,59,62], and comparable to those of the Gd [3], Gd-Si-Ge-based [63–65], La-Fe-Si-based

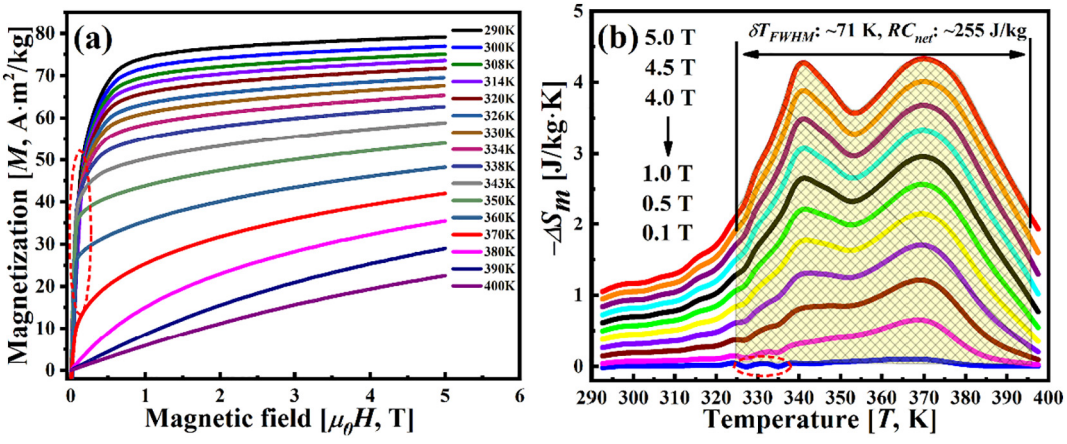


**Fig. 5.** (a) Field-up and field-down isothermal magnetization $M(H)$ curves and (b) temperature dependence of magnetic entropy change $\Delta S_m(T)$ curves at different fields of the bamboo-grained microwires. The red dashed ellipse in (a) displays the intersection of the $M(H)$ curves at low fields. The red dashed ellipse in (b) marks the tiny positive entropy peak at low fields. The double-sided arrow in (b) demonstrates the full width at half maximum $\delta T_{FWHM}$ of the $\Delta S_m(T)$ curve under 5 T. (For interpretation of the references to color in this figure legend, the reader is referred to the web version of this article.)

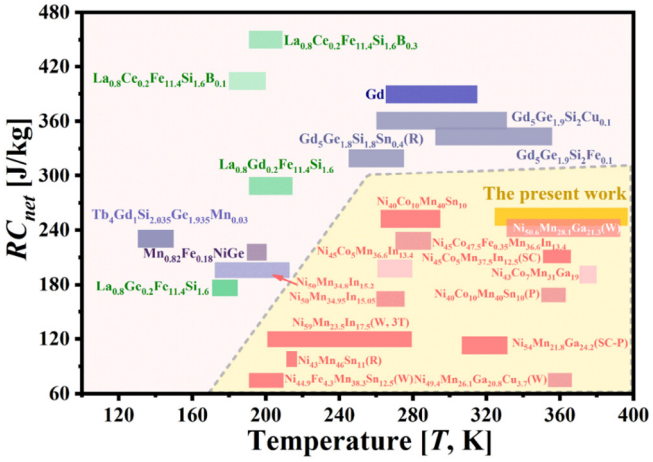


**Fig. 6.** Schematic illustration of the net refrigeration capacity ($RC_{net}$) as a function of temperature under a magnetic field of 5 T for the most studied magnetocaloric materials (Ni-Mn-based [20,21,23,37,55–62], Gd-Si-Ge-based [63–65], La-Fe-Si-based [66,67], Mn-Fe-Ni-Ge compounds [68] and Gd [3]) and the present bamboo-grained microwires. The width of the rectangle indicates the operating temperature interval of each alloy. (W: microwires, P: particles, R: ribbons, SC: single crystal. The dashed line only acts as guide for the eye. For interpretation of the references to color in this figure legend, the reader is referred to the web version of this article.)

[66,67] and Mn-Fe-Ni-Ge [68] magnetocaloric materials. Nevertheless, when compared with rare-earth alloys, the present Ni-Mn-Ga microwires show advantages such as rare-earth free and cost effective. It has been theoretically shown that rod- or wire-shaped magnetic refrigerant materials are more suitable for actual cooling devices than their spherical counterpart, where the refrigerant made of a stack of wires exhibits higher heat transfer coefficient and is more compact than one containing a bed of particles with the same diameter. Besides, better performance can be achieved with reducing the wire diameter, i.e. increasing the heat exchanging area [69]. Furthermore, AC magnetic field is utilized to create thermal cycles in cooling devices, which would induce eddy current and cause uncontrolled heating of the refrigerant material [70]. Small-sized microwires can lower the eddy current thus increase the cooling efficiency [32]. In addition, one dimensional Ni-Mn-Ga microwires possess relatively good mechanical properties [21,35]. Above all, we believe that Ni-Mn-Ga microwire with bamboo-grained structure is a likely candidate for use as magnetic refrigerant either directly used in micro-sized devices or act as building block for macro-sized devices.

## 4. Conclusions

(1) Bamboo-grained microwires with diameter ~30–80 μm, length ~2–20 cm and grain length varying from tens to hundreds of microns were successfully prepared by melt-extraction technique and subsequent high temperature heat treatment at 1323 K for 3 h under 0.5 atm. Argon atmosphere. No obvious preferred grain orientation was obtained in the bamboo-grained microwire at austenite state.

(2) Various martensite variants with fine twin lamella were observed in bamboo-grained microwires. The heterogeneous composition state obtained after high temperature heat treatment is responsible for the multi-variants state.

(3) The martensite structure of the microwires changes from single 7M to a mixture containing 7M and 5M martensite after high temperature heat treatment. Compared with the as-extracted microwires, bamboo-grained ones have both higher martensite transformation temperatures and Curie point.

(4) Enlargement of working temperature interval up to ~71 K under 5 T due to the partly coupled magnetostructural transformation and reduction of the magnetic hysteresis in the bamboo-grained microwires were demonstrated, giving rise to the significantly improved net refrigeration capacity $RC_{net}$ value of 255 J/kg, which is heretofore the largest value reported in Ni-Mn-based Heusler alloys.

## CRediT authorship contribution statement

**M.F. Qian:** Conceptualization, Formal analysis, Writing - original draft, Funding acquisition. **X.X. Zhang:** Conceptualization, Writing - review & editing. **X. Li:** Resources. **R.C. Zhang:** Data curation. **P.G. Martin:** Investigation. **J.F. Sun:** Supervision. **L. Geng:** Supervision. **T.B. Scott:** Writing - review & editing. **H.X. Peng:** Supervision, Writing - review & editing.

## Declaration of competing interest

The authors declare that they have no known competing financial interests or personal relationships that could have appeared to influence the work reported in this paper.

## Acknowledgments

M.F.Q., X.X.Z. and L.G. greatly acknowledge the financial supports from National Natural Science Foundation of China (NSFC) (Grant Number 51701052), Natural Science Foundation of Heilongjiang Province (Grant Number QC2018062), China Postdoctoral Science Foundation (Grant number 2017M620114, 2019T120262) and Heilongjiang Postdoctoral Foundation (Grant number LBH-Z17085), M.F.Q. acknowledges the financial support from theChina Scholarship Council (CSC) for her one year visiting at the University of Bristol under the supervision of Prof. Hua-Xin Peng.

## References

[1] T. Hashimoto, T. Kuzuhara, M. Sahashi, K. Inomata, A. Tomokiyo, H. Yayama, New application of complex magnetic materials to the magnetic refrigerant in an Ericsson magnetic refrigerator, J. Appl. Phys. 62 (1987) 3873.
[2] K.A. Gschneidner, V.K. Pecharsky, D. Fort, Novel thermal effects at the first order magnetic phase transition in erbium, and a comparison with dysprosium, Phys. Rev. Lett. 78 (1997) 4281–4284.
[3] K.A. Gschneidner, V.K. Pecharsky, A.O. Tsokol, Recent developments in magnetocaloric materials, Rep. Prog. Phys. 68 (2005) 1479–1539.
[4] O. Gutfleisch, M.A. Willard, E. Brück, C.H. Chen, S.G. Sankar, J.P. Liu, Magnetic materials and devices for the 21st century: stronger, lighter, and more energy efficient, Adv. Mater. 23 (2011) 821–842.
[5] A. Smith, C.R.H. Bahl, R. Bjørk, K. Engelbrecht, K.K. Nielsen, N. Pryds, Materials challenges for high performance magnetocaloric refrigeration devices, Adv. Energy Mater. 2 (2012) 1288–1318.
[6] V. Franco, J.S. Blázquez, J.J. Ipus, J.Y. Law, L.M. Moreno-Ramírez, A. Conde, Magnetocaloric effect: from materials research to refrigeration devices, Prog. Mater. Sci. 93 (2018) 112–232.
[7] J. Lyubina, R. Schäfer, N. Martin, L. Schultz, O. Gutfleisch, Novel design of La(Fe,Si)$_{13}$ alloys towards high magnetic refrigeration performance, Adv. Mater. 22 (2010) 3735–3739.
[8] P. Gebara, P. Pawlik, Broadening of temperature working range in magnetocaloric La(Fe, Co, Si)$_{13}$-based multicomposite, J. Magn. Magn. Mater. 442 (2017) 145–151.
[9] L.M. Moreno-Ramírez, C. Romero-Muñiz, J.Y. Law, V. Franco, A. Conde, I.A. Radulov, et al., Tunable first order transition in La(Fe,Cr,Si)$_{13}$ compounds: retaining magnetocaloric response despite a magnetic moment reduction, Acta Mater. 175 (2019) 406–414.
[10] V.M. Andrade, N.B. Barroca, A.L. Pires, J.H. Belo, A.M. Pereira, K.R. Pirota, et al., Free-standing and flexible composites of magnetocaloric $Gd_5(Si,Ge)_4$ microparticles embedded in thermoplastic poly(methyl methacrylate) matrix, Mater. Des. 186 (2020) 108354.
[11] K. Rudolph, A.K. Pathak, Y. Mudryk, V.K. Pecharsky, Magnetostructural phase transitions and magnetocaloric effect in $(Gd_{5-x}Sc_x)Si_{1.8}Ge_{2.2}$, Acta Mater. 145 (2018) 369–376.
[12] P. Gebara, Z. Śniadecki, Structure, magnetocaloric properties and thermodynamic modeling of enthalpies of formation of (Mn,X)-Co-Ge (X = Zr, Pd) alloys, J. Alloys Compd. 796 (2019) 153–159.
[13] D. Goswami, K.S. Anand, P.P. Jana, S.K. Ghorai, S. Chattopadhyay, J. Das, Synthesis of a robust multifunctional composite with concurrent magnetocaloric effect and enhanced energy absorption capabilities through a tailored processing route, Mater. Des. (2019) https://doi.org/10.1016/j.matdes.2019.108399.

[14] J.Y. Law, Á. Díaz-García, L.M. Moreno-Ramírez, V. Franco, A. Conde, A.K. Giri, How concurrent thermomagnetic transitions can affect magnetocaloric effect: the $Ni_{49+x}Mn_{36-x}In_{15}$ Heusler alloy case, Acta Mater. 166 (2019) 459–465.
[15] H. Neves Bez, A.K. Pathak, A. Biswas, N. Zarkevich, V. Balema, Y. Mudryk, et al., Giant enhancement of the magnetocaloric response in Ni-Co-Mn-Ti by rapid solidification, Acta Mater. 173 (2019) 225–230.
[16] A. Tekgül, K. Şarlar, İ. Küçük, Changes in structural, magnetic and magnetocaloric properties due to homogenization annealing in $Ni_{54}Mn_{19}Ga_{27}$, J. Magn. Magn. Mater. 469 (2019) 183–188.
[17] H. Sepehri-Amin, A. Taubel, T. Ohkubo, K.P. Skokov, O. Gutfleisch, K. Hono, Microstructural origin of hysteresis in Ni-Mn-In based magnetocaloric compounds, Acta Mater. 147 (2018) 342–349.
[18] Y.H. Qu, D.Y. Cong, S.H. Li, W.Y. Gui, Z.H. Nie, M.H. Zhang, et al., Simultaneously achieved large reversible elastocaloric and magnetocaloric effects and their coupling in a magnetic shape memory alloy, Acta Mater. 151 (2018) 41–55.
[19] D.Y. Cong, L. Huang, V. Hardy, D. Bourgault, X.M. Sun, Z.H. Nie, et al., Low-field-actuated giant magnetocaloric effect and excellent mechanical properties in a NiMn-based multiferroic alloy, Acta Mater. 146 (2018) 142–151.
[20] M.F. Qian, X.X. Zhang, Z.G. Jia, X.H. Wan, L. Geng, Enhanced magnetic refrigeration capacity in Ni-Mn-Ga micro-particles, Mater. Des. 148 (2018) 115–123.
[21] M.F. Qian, X.X. Zhang, L.S. Wei, P. Martin, J.F. Sun, L. Geng, et al., Tunable magnetocaloric effect in Ni-Mn-Ga microwires, Sci. Rep. 8 (2018), 16574.
[22] J. Liu, T. Gottschall, K.P. Skokov, J.D. Moore, O. Gutfleisch, Giant magnetocaloric effect driven by structural transitions, Nat. Mater. 11 (2012) 620–626.
[23] X.X. Zhang, M.F. Qian, Z. Zhang, L.S. Wei, L. Geng, J.F. Sun, Magnetostructural coupling and magnetocaloric effect in Ni-Mn-Ga-Cu microwires, Appl. Phys. Lett. 108 (2016), 052401.
[24] I. Dubenko, M. Khan, A.K. Pathak, B.R. Gautam, S. Stadler, N. Ali, Magnetocaloric effects in Ni-Mn-X based Heusler alloys with X = Ga, Sb, In, J. Magn. Magn. Mater. 321 (2009) 754–757.
[25] V.A. Chernenko, E. Cesari, V.V. Kokorin, I.N. Vitenko, The development of new ferromagnetic shape-memory alloys in Ni-Mn-Ga system, Scr. Mater. 33 (1995) 1239–1244.
[26] R.F. Hamilton, H. Sehitoglu, Y. Chumlyakov, H.J. Maier, Stress dependence of the hysteresis in single crystal NiTi alloys, Acta Mater. 52 (2004) 3383–3402.
[27] J. Liu, T.G. Woodcock, N. Scheerbaum, O. Gutfleisch, Influence of annealing on magnetic field-induced structural transformation and magnetocaloric effect in Ni-Mn-In-Co ribbons, Acta Mater. 57 (2009) 4911–4920.
[28] V. Srivastava, X. Chen, R.D. James, Hysteresis and unusual magnetic properties in the singular Heusler alloy $Ni_{45}Co_5Mn_{40}Sn_{10}$, Appl. Phys. Lett. 97 (2010) 14101.
[29] I. Dubenko, N. Ali, S. Stadler, A. Zhukov, V. Zhukova, B. Hernando, et al., Magnetic, magnetocaloric, magnetotransport, and magneto-optical properties of Ni-Mn-In-based Heusler alloys: bulk, ribbons, and microwires, in: A. Zhukov (Ed.), Novel Functional Magnetic Materials: Fundamentals and Applications, Springer Series in Materials Science, Switzerland 2016, pp. 281–304.
[30] H. Zong, Z. Ni, X. Ding, T. Lookman, J. Sun, Origin of low thermal hysteresis in shape memory alloy ultrathin films, Acta Mater. 103 (2016) 407–415.
[31] Y. Chen, C.A. Schuh, Size effects in shape memory alloy microwires, Acta Mater. 59 (2011) 537–553.
[32] M.F. Qian, X.X. Zhang, L.S. Wei, L. Geng, H.X. Peng, Effect of chemical ordering annealing on martensitic transformation and superelasticity in polycrystalline Ni-Mn-Ga microwires, J. Alloys Compd. 645 (2015) 335–343.
[33] N. Scheerbaum, O. Heczko, J. Liu, D. Hinz, L. Schultz, O. Gutfleisch, Magnetic field-induced twin boundary motion in polycrystalline Ni-Mn-Ga fibres, New J. Phys. 10 (2008), 73002.
[34] P. Zheng, N.J. Kucza, C.L. Patrick, P. Müllner, D.C. Dunand, Mechanical and magnetic behavior of oligocrystalline Ni-Mn-Ga microwires, J. Alloys Compd. 624 (2015) 226–233.
[35] M.F. Qian, X.X. Zhang, L.S. Wei, L. Geng, H.X. Peng, Structural, magnetic and mechanical properties of oligocrystalline Ni-Mn-Ga shape memory microwires, Mater. Today Proc. 2 (2015) S577–S581.
[36] Y. Liu, X. Zhang, D. Xing, H. Shen, D. Chen, J. Liu, et al., Magnetocaloric effect (MCE) in melt-extracted Ni-Mn-Ga-Fe Heusler microwires, J. Alloys Compd. 616 (2014) 184–188.
[37] H. Zhang, M. Qian, X. Zhang, S. Jiang, L. Wei, D. Xing, et al., Magnetocaloric effect of Ni-Fe-Mn-Sn microwires prepared by melt-extraction technique, Mater. Des. 114 (2017) 1–9.
[38] M.F. Qian, X.X. Zhang, C. Witherspoon, J.F. Sun, P. Müllner, Superelasticity and shape memory effects in polycrystalline Ni-Mn-Ga microwires, J. Alloys Compd. 577 (2013) S296–S299.
[39] Y. Boonyongmaneerat, M. Chmielus, D.C. Dunand, Müllner, Increasing magnetoplasticity in polycrystalline Ni-Mn-Ga by reducing internal constraints through porosity, Phys. Rev. Lett. 99 (2007) 247201.
[40] M.F. Qian, X.X. Zhang, L.S. Wei, P.G. Martin, J.F. Sun, L. Geng, et al., Microstructural evolution of Ni-Mn-Ga microwires during the melt-extraction process, J. Alloys Compd. 660 (2016) 244–251.
[41] J. Gutierrez, J.M. Barandiaran, P. Lazpita, C. Segui, E. Cesari, Magnetic properties of a rapidly quenched Ni-Mn-Ga shape memory alloy, Sensors Actuators A Phys. 129 (2006) 163–166.
[42] F. Albertini, S. Besseghini, A. Paoluzi, L. Pareti, M. Pasquale, F. Passaretti, et al., Structural, magnetic and anisotropic properties of $Ni_2MnGa$ melt-spun ribbons, J. Magn. Magn. Mater. 242 (2002) 1421–1424.
[43] L. Righi, F. Albertini, E. Villa, A. Paoluzi, G. Calestani, V. Chernenko, et al., Crystal structure of 7M modulated Ni-Mn-Ga martensitic phase, Acta Mater. 56 (2008) 4529–4535.
[44] C. Seguí, V.A. Chernenko, J. Pons, E. Cesari, V. Khovailo, T. Takagi, Low temperature-induced intermartensitic phase transformations in Ni–Mn–Ga single crystal, Acta Mater. 53 (2005) 111–120.
[45] N. Lanska, O. Soderberg, A. Sozinov, Y. Ge, K. Ullakko, V.K. Lindroos, Composition and temperature dependence of the crystal structure of Ni-Mn-Ga alloys, J. Appl. Phys. 95 (2004) 8074–8078.
[46] Z. Li, K. Xu, Y. Zhang, C. Tao, D. Zheng, C. Jing, Two successive magneto-structural transformations and their relation to enhanced magnetocaloric effect for $Ni_{55.8}Mn_{18.1}Ga_{26.1}$ Heusler alloy, Sci. Rep. 5 (2015), 15143.
[47] O. Heczko, P.S.D. Janickovic, Magnetic properties of Ni-Mn-Ga ribbon prepared by rapid solidification, IEEE Trans. Magn. 38 (2002) 2841–2843.
[48] H. Yan, C.F. Sánchez-Valdés, Y. Zhang, J.L. Sánchez Llamazares, Z. Li, B. Yang, et al., Correlation between crystallographic and microstructural features and low hysteresis behavior in $Ni_{50.0}Mn_{35.25}In_{14.75}$ melt-spun ribbons, J. Alloys Compd. 767 (2018) 544–551.
[49] A. Sozinov, A.A. Likhachev, N. Lanska, K. Ullakko, V.K. Lindroos, 10% magnetic-field-induced strain in Ni-Mn-Ga seven-layered martensite, J. Phys. IV 112 (2003) 955–958.
[50] M. Chmielus, X.X. Zhang, C. Witherspoon, D.C. Dunand, P. Mullner, Giant magnetic-field-induced strains in polycrystalline Ni-Mn-Ga foams, Nat. Mater. 8 (2009) 863–866.
[51] X.X. Zhang, C. Witherspoon, P. Mullner, D.C. Dunand, Effect of pore architecture on magnetic-field-induced strain in polycrystalline Ni-Mn-Ga, Acta Mater. 59 (2011) 2229–2239.
[52] T. Gottschall, A. Gràcia-Condal, M. Fries, A. Taubel, L. Pfeuffer, L. Mañosa, et al., A multicaloric cooling cycle that exploits thermal hysteresis, Nat. Mater. 17 (2018) 929–934.
[53] L. Wei, X. Zhang, W. Gan, C. Ding, L. Geng, Hot extrusion approach to enhance the cyclic stability of elastocaloric effect in polycrystalline Ni-Mn-Ga alloys, Scr. Mater. 168 (2019) 28–32.
[54] V. Recarte, J.I. Pérez-Landazábal, V. Sánchez-Alárcos, V.A. Chernenko, M. Ohtsuka, Magnetocaloric effect linked to the martensitic transformation in sputter-deposited Ni-Mn-Ga thin films, Appl. Phys. Lett. 95 (2009), 141908.
[55] X. Wang, F. Sun, J. Wang, Q. Yu, Y. Wu, H. Hua, et al., Influence of annealing temperatures on the magnetostructural transition and magnetocaloric effect of $Ni_{40}Co_{10}Mn_{40}Sn_{10}$ powders, J. Alloys Compd. 691 (2017) 215–219.
[56] L. Huang, D.Y. Cong, H.L. Suo, Y.D. Wang, Giant magnetic refrigeration capacity near room temperature in $Ni_{40}Co_{10}Mn_{40}Sn_{10}$ multifunctional alloy, Appl. Phys. Lett. 104 (2014), 132407.
[57] D. Bourgault, J. Tillier, P. Courtois, D. Maillard, X. Chaud, Large inverse magnetocaloric effect in $Ni_{45}Co_5Mn_{37.5}In_{12.5}$ single crystal above 300 K, Appl. Phys. Lett. 96 (2010), 132501.
[58] L. Chen, F.X. Hu, J. Wang, L.F. Bao, J.R. Sun, B.G. Shen, et al., Magnetoresistance and magnetocaloric properties involving strong metamagnetic behavior in Fe-doped $Ni_{45}(Co_{1-x}Fex)_5Mn_{36.6}$ $In_{13.4}$ alloys, Appl. Phys. Lett. 101 (2012), 012401.
[59] S. Fabbrici, J. Kamarad, Z. Arnold, F. Casoli, A. Paoluzi, F. Bolzoni, et al., From direct to inverse giant magnetocaloric effect in Co-doped NiMnGa multifunctional alloys, Acta Mater. 59 (2011) 412–419.
[60] V. Vega, L. Gonzalez, J. Garcia, W.O. Rosa, D. Serantes, V.M. Prida, et al., $Ni_{59.0}Mn_{23.5}In_{17.5}$ Heusler alloy as the core of glass-coated microwires: magnetic properties and magnetocaloric effect, J. Appl. Phys. 112 (2012), 033905.
[61] Y. Zhang, Q. Zheng, W. Xia, J. Zhang, J. Du, A. Yan, Enhanced large magnetic entropy change and adiabatic temperature change of $Ni_{43}Mn_{46}Sn_{11}$ alloys by a rapid solidification method, Scr. Mater. 104 (2015) 41–44.
[62] A.K. Pathak, M. Khan, I. Dubenko, S. Stadler, N. Ali, Large magnetic entropy change in $Ni_{50}Mn_{50-x}In_x$ Heusler alloys, Appl. Phys. Lett. 90 (2007), 262504.
[63] T. Zhang, Y. Chen, Y. Tang, The magnetocaloric effect and hysteresis properties of melt-spun $Gd_5Si_{1.8}Ge_{1.8}Sn_{0.4}$ alloy, J. Phys. D: Appl. Phys. 40 (2007) 5778–5784.
[64] R.D. Shull, V. Provenzano, A.J. Shapiro, A. Fu, M.W. Lufaso, J. Karapetrova, et al., The effects of small metal additions (Co,Cu,Ga,Mn,Al,Bi,Sn) on the magnetocaloric properties of the $Gd_5Ge_2Si_2$ alloy, J. Appl. Phys. 99 (2006) 08K908.
[65] J.X. Min, X.C. Zhong, V. Franco, H.C. Tian, Z.W. Liu, Z.G. Zheng, et al., Structure, magnetic properties and giant magnetocaloric effect of $Tb_4Gd_1Si_{2.035}Ge_{1.935}Mn_{0.03}$ alloy, Intermetallics 57 (2015) 68–72.
[66] P. Shamba, J.C. Debnath, R. Zeng, J.L. Wang, S.J. Campbell, S.J. Kennedy, et al., Reduction of hysteresis losses in the magnetic refrigerant $La_{0.8}Ce_{0.2}Fe_{11.4}Si_{1.6}$ by the addition of boron, J. Appl. Phys. 109 (2011) 07A940.
[67] P. Shamba, R. Zeng, J.L. Wang, S.J. Campbell, S.X. Dou, Enhancement of the refrigerant capacity in low level boron doped $La_{0.8}Gd_{0.2}Fe_{11.4}Si_{1.6}$, J. Magn. Magn. Mater. 331 (2013) 102–108.
[68] R. Wu, F. Shen, F. Hu, J. Wang, L. Bao, L. Zhang, et al., Critical dependence of magnetostructural coupling and magnetocaloric effect on particle size in Mn-Fe-Ni-Ge compounds, Sci. Rep. 6 (2016), 20993.
[69] D. Vuarnoz, T. Kawanami, Numerical analysis of a reciprocating active magnetic regenerator made of gadolinium wires, Appl. Therm. Eng. 37 (2012) 388–395.
[70] A.M. Aliev, A.B. Batdalov, L.N. Khanov, V.V. Koledov, V.G. Shavrov, I.S. Tereshina, et al., Magnetocaloric effect in some magnetic materials in alternating magnetic fields up to 22Hz, J. Alloys Compd. 676 (2016) 601–605.